Journal of Environmental Health Science and Engineering (2023) 21:93–105
https://doi.org/10.1007/s40201-022-00842-x

RESEARCH ARTICLE

Design and preparation of amino-functionalized core-shell magnetic nanoparticles for photocatalytic application and investigation of cytotoxicity effects

Zahra Sabouri[1,2] · Mohammad Sabouri[3] · Samaneh Sadat Tabrizi Hafez Moghaddas[1] · Majid Darroudi[1,4,5]

Received: 3 July 2022 / Accepted: 13 November 2022 / Published online: 30 November 2022

Abstract

The goal of the current paper was a synthesis of Amino-functionalized Fe_3O_4@SiO_2 core-shell magnetic nanoparticles as a unique efficient photocatalyst for removing organic dyes from aqueous environments. The magnetic Fe_3O_4@SiO_2 core-shell was produced by a silica source to avoid aggregation by the co-precipitation method. Next, functionalized by using 3-Aminopropyltriethoxysilane (APTES) via a post-synthesis link. The chemical structure, magnetic properties, and shape of the manufactured photocatalyst (Fe_3O_4@SiO_2-NH_2) were described by XRD, VSM, FT-IR, FESEM, EDAX, and DLS/Zeta potential analyses. The XRD findings approved the successful synthesis of nanoparticles. The photocatalytic activity of Fe_3O_4@SiO_2-NH_2 nanoparticles was examined for MB degradation and the degradation performance was about 90% in the optimum conditions. Also, the cytotoxicity of Fe_3O_4, Fe_3O_4@SiO_2 core-shell, and Fe_3O_4@SiO_2-NH_2 nanoparticles was examined on CT-26 cells using an MTT assay, the finding has shown that nanoparticles can be used for inhibiting cancer cells.

Keywords Core-shell · Magnetic nanoparticles · Photocatalyst · Co-precipitation · Cytotoxicity

Introduction

Photocatalytic processes have been used for many years as one of the environmental solutions in the industrialized countries of the world. Meanwhile, new photocatalytic materials with different properties enter the market every day and are used [1]. Nanotechnology promises a very broad future for this field by creating a new approach to the photocatalytic industry [2]. The importance of nanostructured materials at the nanoscale show different chemical and physical properties of the bulk of the matter [3]. In addition to the difference in their bulk properties, in this area, the properties of the material are related to their size and shape [4]. By making changes in the shape and size of nanostructures can be obtained materials with new properties [5]. Overall the recent decades, magnetic nanoparticles have been attended by a range of scientific disciplines as they possess high potential in various application fields such as chemistry, biology, and medicine [6]. The Fe_3O_4 nanoparticles display high magnetic saturation, stability, and biocompatibility on the surface of the nanoparticles that can be applied for an extensive range of purposes [7]. The Fe_3O_4 nanostructured photocatalysts with high photocatalytic properties are one of the key technologies in controlling environmental pollution because of their very high surface-to-volume ratio. This technology can be used in water, wastewater, and air treatment systems and provide a healthy environment by eliminating chemical pollution [8]. The application of nanotechnology and using of inorganic supplies as catalysts in eliminating chemical pollution is one of the benefits of chemistry green. In recent times, among several catalysts, the variation of Fe_3O_4 nanoparticles with organic and inorganic combinations obtained special attention [9]. The Fe_3O_4

✉ Majid Darroudi
majiddarroudi@gmail.com; darroudim@mums.ac.ir

1 Department of Medical Biotechnology and Nanotechnology, Faculty of Medicine, Mashhad University of Medical Sciences, Mashhad, Iran

2 Medical Toxicology Research Center, Faculty of Medicine, Mashhad University of Medical Sciences, Mashhad, Iran

3 School of Civil Engineering, University of Science and Technology (UST), Tehran, Iran

4 Nuclear Medicine Research Center, Mashhad University of Medical Sciences, Mashhad, Iran

5 Department of Basic Medical Sciences, Neyshabur University of Medical Sciences, Neyshabur, Iran

nanoparticles contain particular attributes containing: easy separation, low cost, simple synthesis, great stability, and high surface area [10]. Researchers have recently concentrated on the synthesis of Fe_3O_4 nanoparticles by implementing a variety of pathways to regulate their size, shape, and morphology with adjustable and desirable properties [11]. A variety of synthesis routes have been reported for the preparation of these magnetic nanoparticles, such as co-precipitation, hydrothermal, and micro-emulsion. Fe_3O_4 nanoparticles were used in various fields such as biosensors and as a catalyst in the removal of organic dyes from wastewater [12, 13]. The Fe_3O_4 nanoparticles suffer from a variety of major problems, such as fast agglomeration and extensive surface area, causing magnetism loss [14]. Consequently, surface modification of Fe_3O_4 nanoparticles is essential to avoid the problems referred to above [15]. The coating is the most common process of surface modification for connecting organic or inorganic compounds on the surface of Fe_3O_4 nanoparticles. The functionalization of magnetic nanoparticles will boost their physicochemical attributes, creating suitable candidates for photocatalysis or biomedicinal applications [10]. The core-shell compounds are one notable structure wherein a SiO_2 layer was put on the core surface. The SiO_2 shell is the most common sample for creating core-shell structures with Fe_3O_4. SiO_2 has used due to its great thermal stability and its surface properties, and it can keep OH groups on the surface. Thus, in this study, the Fe_3O_4 nanoparticles were used as a core covered by a SiO_2 shell and modified by amino groups for the synthesis of the $Fe_3O_4@SiO_2$-NH_2 as an effective nano magnetic photocatalyst. Initially, Fe_3O_4 nanoparticles were manufactured by the usage of a co-precipitation process and then covered via the SiO_2 layer. The covered nanoparticles were functionalized thru APTES. Synthesis of surface-modified magnetite nanoparticles and subsequent functionalization has been confirmed by the usage of FTIR, XRD, FESEM/EDX/PSA, DLS/Zeta potential, and VSM analyses. The aim of the current study was to evaluate the photocatalytic activity of the synthesized $Fe_3O_4@SiO_2$-NH_2 nanoparticles to decompose the MB dye under UV-A light for the first time. In continuation, the cytotoxicity effect of Fe_3O_4, $Fe_3O_4@SiO_2$ core-shell, and $Fe_3O_4@SiO_2$-NH_2 nanoparticles were assessed on CT-26 cell lines using the MTT test. Functionalization and examination these applications show the novelty of our work.

Experimental

Chemicals

Ferrous chloride ($FeCl_2.4H_2O \geq 99\%$), Ferric chloride ($FeCl_3.6H_2O \geq 99\%$), ethanol ($CH_3CH_2OH \geq 99.9\%$), ammonia (30%), 3-Aminopropyltriethoxysilane (APTES), and Tetraethyl orthosilicate (TEOS ≥ 99.0%) have been purchased of Merck Co.

Synthesis of Fe_3O_4 nanoparticles

For the synthesis of Fe_3O_4 nanoparticles with the co-precipitation method, briefly, $FeCl_2.4H_2O$ and $FeCl_3.6H_2O$ salts with a molar proportion of 1:2 have been dissolved in distilled water (50.0 mL) and were stirred with vigorous magnetic under a nitrogen atmosphere. Next, ammonium hydroxide solution (20.0 mL NH_4OH, 2 M) was added dropwise with continuous stirring and the temperature of the mixture has been reached 45 °C and maintained for 1 h. The resulting Fe_3O_4 black precipitates were washed several times with ethanol and water and dried by freeze-drying for 48 h at -80 °C [16, 17].

Preparation of $Fe_3O_4@SiO_2$ core-shell

For the preparation of $Fe_3O_4@SiO_2$ Core-shell, Fe_3O_4 nanoparticles (0.50 g) have been dispersed in a solution, which involved water (10.0 mL), ethanol (30.0 mL), and ammonia (1.0 mL) under a nitrogen atmosphere. This mixture solution was sonicated for 30.0 min at 25 °C, later, 4.0 mL of ethanol that was accompanied by 1.0 mL of TEOS was added to the solution drop wisely while vigorously stirring for 24 h at 25 °C to create a dark-brown suspension. The $Fe_3O_4@SiO_2$ core shell was washed several times with ethanol and water and dried by the use of freeze-drying for 48 h at -80 °C.

Surface modification of $Fe_3O_4@SiO_2$ core-shell with APTES

$Fe_3O_4@SiO_2$-NH_2 nanoparticles have been synthesized by inducing a reaction between $Fe_3O_4@SiO_2$ core-shell and APTES within ethanol. Initially, the synthesized $Fe_3O_4@SiO_2$ core-shell (0.15 g) was dispersed in ethanol (20.0 mL) and sonicated for 20 min, thereafter, the APTES (500.0 µL) was added to the solution drop wisely and stirred with magnetic stirring for 24 h at 25 °C. The next achievement of the reaction, the $Fe_3O_4@SiO_2$-NH_2 precipitate was washed several times with water and dried by freeze-drying for 48 h at -80 °C [11, 18]. Schematic synthesis of $Fe_3O_4@SiO_2$-NH_2 nanoparticles was displayed in Fig. 1.

Photocatalytic test of $Fe_3O_4@SiO_2$-NH_2 nanoparticles for MB degradation

The photocatalytic activity of the synthesized $Fe_3O_4@SiO_2$-NH_2 nanoparticles was assessed for MB dye degradation. First, the 10.0 mg $Fe_3O_4@SiO_2$-NH_2 nanoparticles were immersed in a 100.0 mL solution containing 1.0 mg of MB

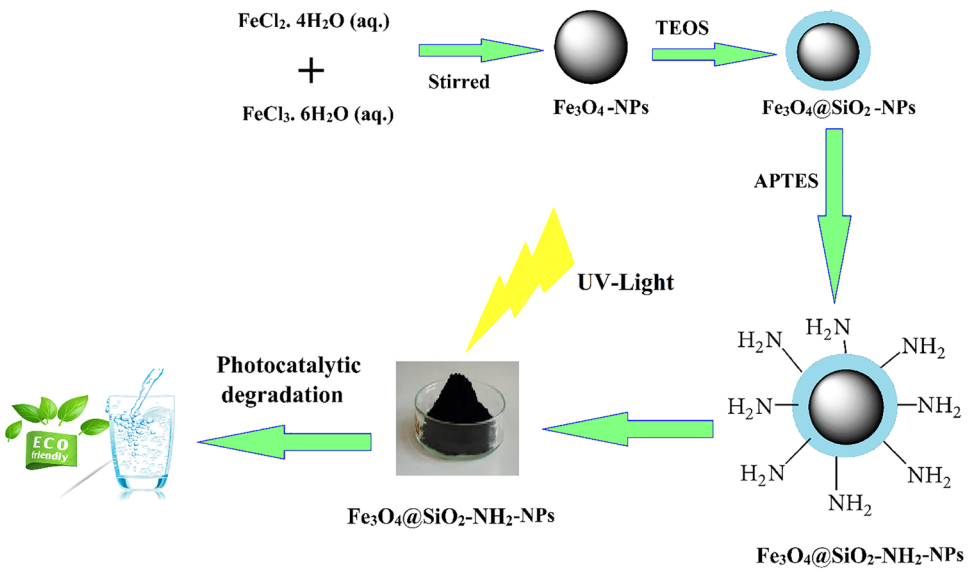

Fig. 1 The preparation schematic of Fe_3O_4@SiO_2-NH_2 nanoparticles

under optimum conditions (pH:11) and were exposed under UVA (11 W) light irradiated while stirring the solution. To examine, the dye degradation percentage, the absorbance was measured at intervals of 25 min by the usage of the UV-Vis spectrophotometer and repeated for up to 150 min.

Results and discussion

Characterization

The Fe_3O_4, Fe_3O_4@SiO_2 core-shell, and Fe_3O_4@SiO_2-NH_2 nanoparticles were analyzed by Fourier transform infrared spectrophotometer (8400-SHIMADZU) to determine the functional groups. The crystalline structure of the nanoparticles was examined using of XRD pattern (D8-Advance Bruker). The morphology and size of nanoparticles were determined using FESEM/EDAX/PSA (TESCAN BRNO-Mira3 LMU) images and Image software. Zeta potential measurements were used to examine the stability of the colloidal suspension and the size distribution of nanoparticles was evaluated by the means of DLS (by Cordovan, France) at neutral pH. The optical features of samples were examined with the usage of UV-Vis spectroscopy (UV-Vis 2550-SHIMADZU). The VSM (MDKB model) analysis was used to investigate superparamagnetic behavior.

Photocatalytic activity of Fe_3O_4@SiO_2-NH_2nanoparticles

The photocatalytic manner demonstrates a vital role in the refinement of contaminated water. In this respect, Fe_3O_4@SiO_2-NH_2 nanoparticles have been applied as the catalyst for the MB dye degradation below UV-A light. The MB dye degradation without catalyst was investigated in the presence of UVA (11 W) light, results showed that MB dye without catalyst was very hard and was decomposed, as proved in Fig. 2a. The percentage of dye degradation was determined using Eq. 1 which was 18% after 150 min [19]. Also, photocatalytic degradation of MB dye was done in the presence of Fe_3O_4@SiO_2-NH_2 nanoparticles under UVA (11 W) light in optimum conditions. The photocatalytic activity curve of Fe_3O_4@SiO_2-NH_2 nanoparticles in MB dye decomposition is displayed in Fig. 2b. The MB absorbance was decreased by increasing the time of irradiation, and the performance efficiency increased with increasing reaction time [20, 21]. The dye degradation percentage was 90% after 150 min.

$$\text{Degradation}(\%) = \frac{A_0 - A_t}{A_0} \times 100 \quad (1)$$

According to the outcomes of the photocatalytic investigations, the reaction kinetics was studied. The results of kinetic studies showed that the photocatalytic process follows the first-order kinetics that is proved in Eq. 2 with $R^2 = 0.9947$ and the reaction rate constant is $k_{obs} = 0.0134\ min^{-1}$. The examinations kinetics of MB degradation using Fe_3O_4@SiO_2-NH_2 nanoparticles were presented in Fig. 3.

$$Ln\left(\frac{C_t}{C_0}\right) = K_{obs}t \quad (2)$$

According to the obtained outcomes, the seen photocatalytic activity on the removal of MB dye was wholly satisfying, as the synthesized nanoparticles were able to be degraded by more than 90% of MB dye in aqueous solutions. Following the work of Xuan et al., magnetic nanoparticles can stand as a promising photocatalyst [22]. Also, Xinman et al. examined

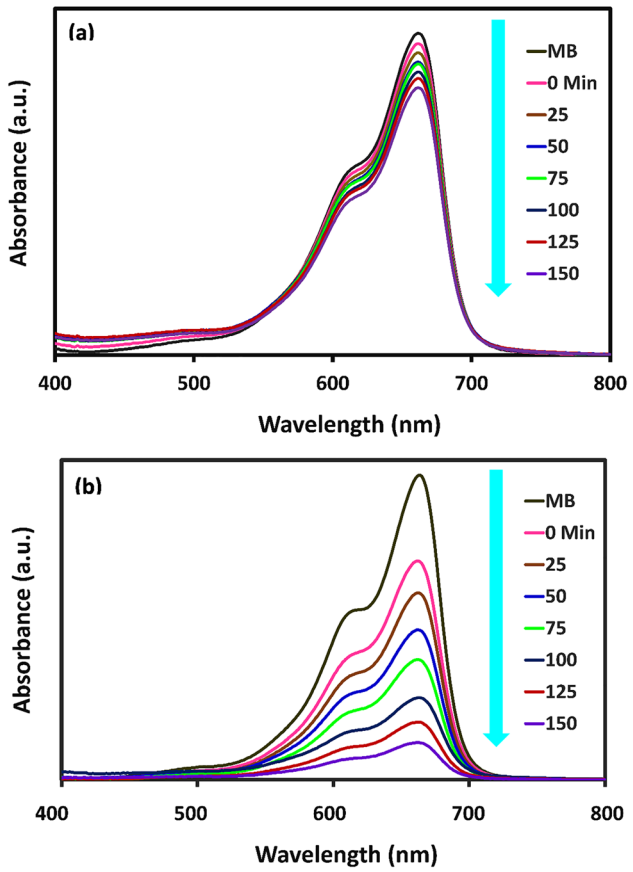

Fig. 2 Decomposition of MB dye in the absence of Fe_3O_4@SiO_2-NH_2 nanoparticles (**a**) Decomposition of MB dye using Fe_3O_4@SiO_2-NH_2 nanoparticles under UVA light irradiation (**b**)

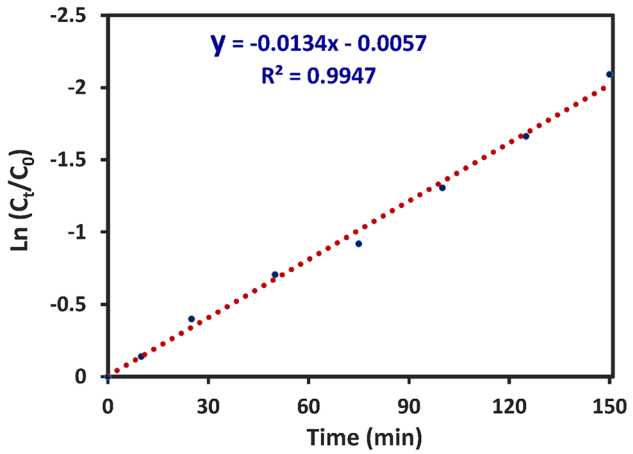

Fig. 3 The examinations kinetics of MB degradation using Fe_3O_4@SiO_2-NH_2 nanoparticles

the photocatalyst activity of the magnetical heterostructures under visible light for the reduction of heavy metal ions [23]. In other research, Yuan et al. reported the photocatalyst activity of the magnetic composite for the degradation of Rhodamine B (RhB) dye [24]. Jiang et al. also studied the photocatalyst activity of the magnetic composite for the degradation of RhB dye under visible light [25]. By comparing the outcomes was observed that synthesized amino-functionalized core-shell magnetic nanoparticles have a more photocatalytic effect in comparison with other nanoparticles [22]. Magnetic nanoparticles are currently the subject of various studies due to their potential applications in the treatment of water and wastewater. Magnetite nanoparticles widely are applied as catalysts due to their advantages such as small size, low toxicity, and unique superparamagnetic. There are significant concerns about nanoparticles that may have long-term toxic effects. To overcome these problems, NH_2-functionalized Fe_3O_4/SiO_2 nanoparticles can reduce long-term toxic effects. Moreover, NH_2-functionalized Fe_3O_4/SiO_2 nanoparticles are a promising substance for the removal of organic dyes from different industries.

Photocatalytic activity mechanism

The photocatalyst mechanism of MB dye degradation is displayed in Fig. 4. The MB is a nitrogen-containing aromatic compound ($C_{16}H_{18}N_3SCl$). Electron-hole ($h^+ - e^-$) pairs are formed due to UVA-light radiation to iron oxide nanoparticles. This electron–hole causes to oxidize/reduces the organic pollutant (MB dye). Electrons (e^-) react with oxygen molecules (O_2) during a reduction reaction to product anionic superoxide radical ($O_2^{\circ-}$), and the produced holes react with H_2O molecules during an oxidation reaction to produce hydroxyl radicals (OH°). These two produced radicals are very highly reactive species and contain sufficient energy and react with organic pigments and various contaminants to cause them to decompose [26]. By breaking the dye molecule bonds and their decomposition, their toxic and dangerous properties are lost and the produced products are non-toxic than raw materials. In 2012, W. Wu et al. investigated the photocatalytic activity of Fe_2O_3/ZnO core-shell to degradation of Rhodamin B dye. They found that the photocatalytic activity of heterostructures could be greatly improved by pairing them with other semiconductors such as ZnO [27]. The outcomes are similar to the other literature results. The mechanism of photocatalytic reactions of Fe_3O_4@SiO_2-NH_2 nanoparticles is given by the following reactions (3 to 8) [22].

$$hv(UV) + Fe_3O_4@SiO_2 - NH_2 \rightarrow h^+ + e^- \quad (3)$$

$$H_2O + h^+ \rightarrow H^+ + OH^\circ \quad (4)$$

$$O_2 + e^- \rightarrow O_2^{\circ-} \quad (5)$$

$$Dye + h^+ \rightarrow Oxidation\ products \quad (6)$$

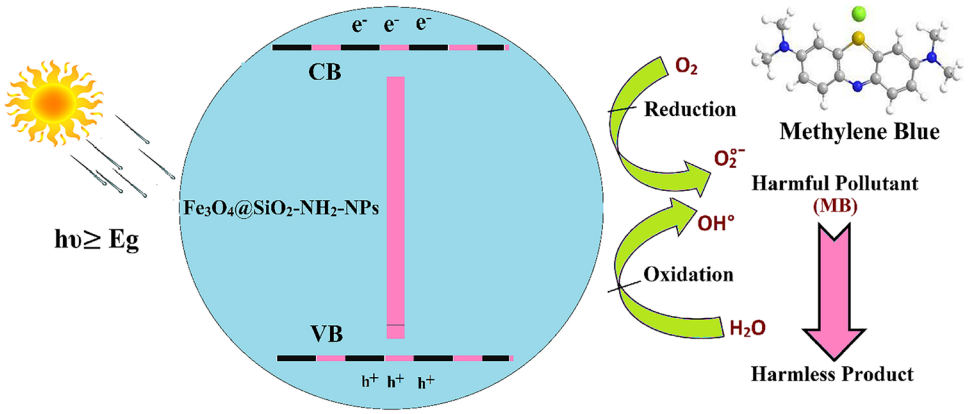

Fig. 4 The schematic mechanism of MB dye degradation by using Fe_3O_4@SiO_2-NH_2 nanoparticles

$$Dye + e^- \rightarrow Reduction\ products \quad (7)$$

$$Dye + OH^{\circ}/O_2^{\circ -} \rightarrow Degradation\ products \quad (8)$$

Investigation of different parameters on MB degradation using Fe_3O_4@SiO_2-NH_2 nanoparticles

To regulate the optimal condition of MB dye degradation by Fe_3O_4@SiO_2-NH_2 nanoparticles investigates have been done at various concentrations of photocatalyst (Fe_3O_4@SiO_2-NH_2 nanoparticles: 3, 6, and 10 mg L^{-1}), various amounts of dye (MB: 1, 3, and 5 mg L^{-1}), and different pH (3, 7, and 11).

pH

As pH is an important parameter affecting photocatalytic degradation. The current study has investigated the optimization of pH parameters. For this goal, the pH range (3, 7, and 11) in MB (1 mg L^{-1}) and the catalyst concentrations (10 mg L^{-1}) were assessed under UVA light (11 W) at the interval of 25 min. The degradation percentage was calculated by the usage of Eq. (1). The outcomes of MB degradation at various pH were presented in Fig. 5a. As

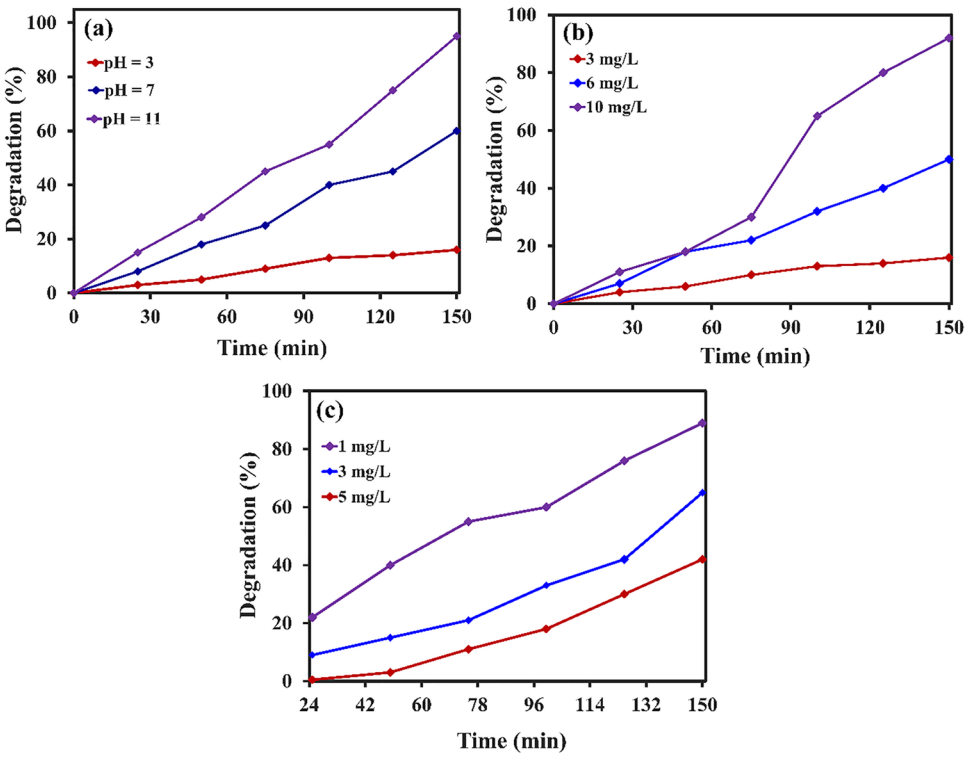

Fig. 5 Influence of pH (**a**), photocatalyst concentration (**b**), and dye concentration in MB dye degradation with UV/Fe_3O_4@SiO_2-NH_2 nanoparticles system (**c**)

seen in Fig. 5a, the dye degradation percentage was raised in the basic medium and decreased in the acidic medium. The MB degradation percentages in the pH of 3, 7, and 11 were about 19, 60, and 91% respectively. The pH influence can be described by the MB dye nature. As MB dye has a cationic nature, it can be concluded that increasing the pH and negative level of the catalyst is useful in the degradation of dye [28]. By increasing the pH, more hydroxyl radicals (OH°) or superoxide anion radicals ($O_2^{\circ-}$) are produced, as a result, reactions occur more quickly among created radicals and MB molecules and then, the MB dye decomposes into different compounds such as CO_2, nitrogen, and sulfur [29]. The outcomes of the current study correspond to the work of Zhihui et al. [30].

Concentration of catalyst

To reach the optimum quantity of catalyst, numerous investigations were finalized in different concentrations. The first standard solution was organized at a pH of 11, MB value equal to 1.0 mg L^{-1}, and various concentrations of catalyst (3, 6, and 10 mg L^{-1}) under UVA light (11 W). The adsorption of the solution was read usage of UV-Vis spectrophotometry. The degradation performance was estimated by the usage of Eq. (1). According to obtained results, it was found that with increasing the concentrations of catalyst (3, 6, and, 10 mg L^{-1}), the degradation percentage of MB was increased (18, 50, and 90%) respectively. conclusions of MB degradation at different concentrations are displayed in Fig. 5b. The detected increase in the reaction of rate was correlated with the rise in the active sites on the level of the catalyst and the rise in photons [28].

Concentration of dye

The findings of various amounts of MB (1, 3, and 5 mg L^{-1}) at pH of 11 and catalyst concentration of 10 mg L^{-1} are displayed in Fig. 5c. The outcomes have displayed that via raising the MB value (1, 3, and 5 mg L^{-1}) the degradation performance was decreased (90, 64, and 42%) respectively. The reduction of degradation performance could be caused to reduced active positions of the catalyst, which is created for the production of OH°. Therefore, by increasing concentration, MB molecules connected to the surface of nanoparticles inhibit the production of OH°. The results matched the study of Jazini Zadeh et al. [31].

FTIR

FTIR technique was used to evaluate the purity and existence of functional groups and chemical bonds of the synthesized nanoparticles in the range from 4000 to 400 cm^{-1}. The FTIR spectrum of Fe_3O_4, Fe_3O_4@SiO_2 core-shell, and Fe_3O_4@SiO_2-NH_2 nanoparticles was demonstrated in Fig. 6. As presented in Fig. 6. the FTIR spectrum of Fe_3O_4 nanoparticles exhibit peaks at 588, 1621, and 3446 cm^{-1} that were linked to the presence of the Fe-O bond, bending vibration, and stretching vibration of O-H respectively. The FTIR finding approved that the nanoparticles contained Fe_3O_4; these bands were seen in all synthesized samples, denoting the existence of Fe_3O_4 nanoparticles in all steps. The Fe_3O_4@SiO_2 core-shell spectrum demonstrations bands at 1074 and 3350 cm^{-1}. The detected peak at 1074 cm^{-1} is related to Si-O-Si vibrations, which approve the existence of SiO_2 coatings in the core-shell [32]. The achieved results matched the work of Ghasemzadeh *et al* [33]. The observed band at 3350 cm^{-1} relates to -OH groups on the magnetite surface. These outcomes demonstrated that the Fe_3O_4 nanoparticles were coated with SiO_2 successfully. As shown in Fig. 6, the Fe_3O_4@SiO_2 core-shell functionalized via APTES was confirmed with the FTIR spectrum. Successful functionalization of Fe_3O_4@SiO_2 core-shell recorded at 3400 and 1592 cm^{-1} that linked to the stretching and bending vibrations of amino groups. The detected strip at 1039 cm^{-1} is related to Si-O-Si stretching vibrations. The outcomes approve the manufacture of silica shells on the Fe_3O_4 surface and the amino-functionalization of the Fe_3O_4@SiO_2 core-shell [34]. The present results were matched via the work of Zhang *et al*. and exhibited different functional groups in synthesized nanoparticles [35]. Thus, it was shown by the FT-IR outcomes that the nanoparticles were synthesized successfully via the co-precipitation method.

XRD pattern

The crystalline structures and composition of the prepared nanoparticles were primarily recognized using XRD. XRD

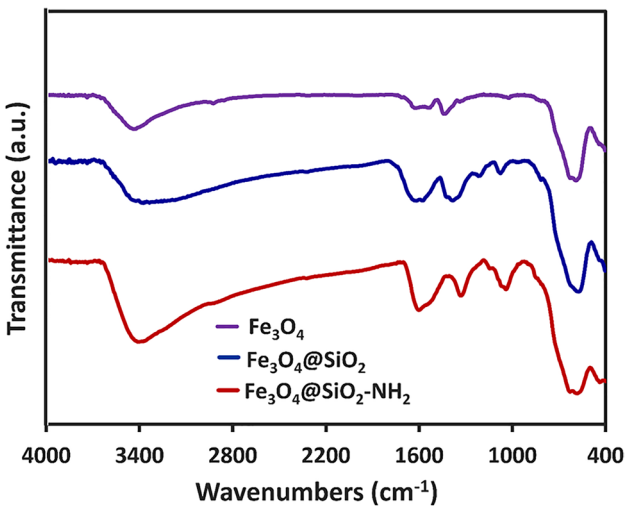

Fig. 6 FTIR spectrum of synthesized nanoparticles

Table 1 Comparison of particle size of the samples

NPs	Fe_3O_4	Fe_3O_4@SiO_2	Fe_3O_4@SiO_2-NH_2
FWHM (Rad.)	0.236	0.708	0.344
2Theta (Deg.)	35.60	35.62	35.62
Crystallite size (nm)	35	20	24

Table 2 The Zeta potential and DLS results of Fe_3O_4, Fe_3O_4@SiO_2 core-shell, and Fe_3O_4@SiO_2-NH_2 nanoparticles

NPs	Fe_3O_4	Fe_3O_4@SiO_2	Fe_3O_4@SiO_2-NH_2
Zeta potential (mV)	-13.03	-15.01	-13.26
Z-Average (nm)	45	64	126
Polydispersity Index (PDI)	0.164	0.328	0.233

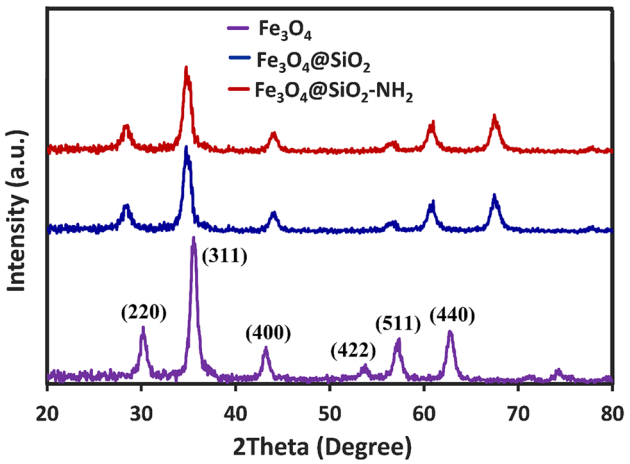

Fig. 7 The XRD patterns of synthesized nanoparticles

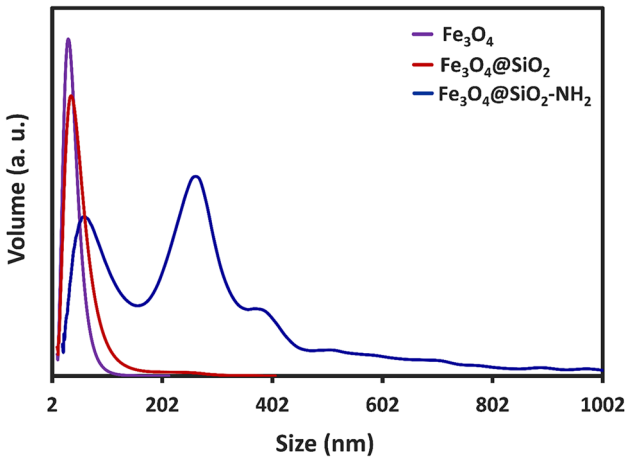

Fig. 8 DLS analyses of synthesized nanoparticles

patterns of nanoparticles were presented in Fig. 7. The detected peaks in the Fe_3O_4 spectrum follow the XRD pattern of standard Fe_3O_4 with the greatly crystalline and cubic spinel structure of Fe_3O_4 nanoparticles [10]. The detected peaks at $2\theta = 30.2°$, 35.6°, 43.1°, 53.7°, 57.2°, and 62.9° were apportioned to (220), (311), (400), (422), (511), and (440) reflectance, respectively that are well-matched with JCPDS # 65–3107 [36]. The same set of mentioned peaks was seen in the XRD figures of Fe_3O_4@SiO_2 core-shell and Fe_3O_4@SiO_2-NH_2 nanoparticles. No apparent change was detected in the XRD pattern after silica coating, indicating that the formed silica shell on the face of the magnetite was amorphous [18, 37]. This suggests that the Fe_3O_4@SiO_2 core-shell was manufactured well with no harm to the crystal structure of the Fe_3O_4 core. Also, as demonstrated during the coating and modification process, the crystallinity or crystal structure of the nanoparticles was not changed, representing the surface modification of the Fe_3O_4 nanoparticles didn't influence the physical attributes of the magnetite materials [8]. Similar to the attained results of Mohammad et al., nanoparticles were synthesized successfully by the usage of the co-precipitation method. In another work, Chao et al. reported Fe_3O_4@SiO_2 core-shell to size 20 nm that the nanoparticles were made of crystalline [38]. The crystallite size of nanoparticles was estimated via the Debye-Scherrer equation (Eq. 9) [39]. Fabrication of the crystalline structure of nanoparticles was approved via the XRD pattern and was comparable to the work of Zhang et al., [35].

$$\mathcal{D} = \frac{k\lambda}{\beta \cos\theta} \tag{9}$$

where D is size, K is equal to 0.9, λ is equal to 0.154 nm, β is the width of the peak in half-maximum, and θ is the angle. The crystallite size of nanoparticles was presented in Table 1 which is in agreement with the FESEM/PSA results. Also, the results of the current study are in agreement with the research of Ghasemzadeh et al. [18].

DLS and Zeta potential

The hydrodynamic diameter changes of Fe_3O_4, Fe_3O_4@SiO_2 core-shell, and Fe_3O_4@SiO_2-NH_2 nanoparticles were assessed by the usage of DLS analysis. DLS curves of nanoparticles were displayed in Fig. 8. The gained Z-averages and polydispersity index (PDI) were 45 (0.164), 126 (0.328), and 64 (0.233) nm respectively. Although FESEM/PSA images and XRD patterns of nanoparticles were shown of low aggregation. On the other, the hydrodynamic size of the Fe_3O_4@SiO_2 core-shell was larger than its crystallite size.

The core-shell manufacture and presence of amine groups in the composition of Fe_3O_4@SiO_2-NH_2 nanoparticles caused a notable increase in the hydrodynamic sizes [8]. The hydrodynamic size of nanoparticles was influenced by the created Hydrogen bonds with water, which cause to increase in the size of particles [11]. The clustering more than of how many particles can be another probable explanation for this view. The zeta potentials were reported at pH: 7. The negative zeta potentials were presented for all the nanoparticles in the aqueous medium, which is a sign of particle stability. The Z-averages and polydispersity index (PDI) and zeta potential of nanoparticles were presented in Table 2. Similar to the attained results of Xueling et al., the narrow peaks of our work show that the Fe_3O_4@SiO_2-NH_2 nanoparticles were monodispersed [40].

FESEM/PSA/EDAX analysis

The shape and size of synthesized nanoparticles were described using FESEM/PSA/ EDAX analysis. The FESEM images of the synthesized Fe_3O_4, Fe_3O_4@SiO_2 core-shell, and Fe_3O_4@SiO_2-NH_2 nanoparticles in different scales (200 and 500 nm, and 1 µm) were shown in Fig. 9a-c, e-g, i-k respectively. The synthesized Fe_3O_4 nanoparticles exhibited spherical shapes with uniform distribution. The FESEM image of the synthesized Fe_3O_4@SiO_2 core-shell was observed spherical with the SiO_2 layer and this layer was considered to consist of SiO_2 [41]. Also, the FESEM images of Fe_3O_4@SiO_2-NH_2 nanoparticles showed a spherical shape after surface modification and these match with the FT-IR and XRD outcomes. The core (Fe_3O_4) and shell (SiO_4) structure of the nanoparticles was clear in FESEM images. The rise in particle size next to coating via SiO_2 and surface modification with NH_2 groups was further confirmed by FESEM micrographs using ImageJ®. The PSA curves displayed that the particle size of Fe_3O_4@SiO_2 core-shell (Fig. 9h, 45.4 nm) was bigger than those functionalized Fe_3O_4@SiO_2 by NH_2 groups (Fig. 9l, 39.3 nm), and Fe_3O_4 (Fig. 9d, 39.1 nm). The EDX analysis demonstrated that the atomic composition of the Fe and O elements in Fe_3O_4 nanoparticles was 41.11 and 58.89%, respectively (Fig. 9m). Additionally, the atomic percentage of O, Si, and Fe in the Fe_3O_4 nanoparticles coated with SiO_2 were 62.21, 9.51, and 28.28% respectively (Fig. 9n). Also, the atomic percentage of O, Si, N, and Fe in the Fe_3O_4@SiO_2-NH_2 nanoparticles was 69.28, 7.82, 6.9, and 16% respectively (Fig. 9o). The atomic and weight percentages of elements are presented in Table 3. The synthesized nanoparticles were wholly dispersed in the solution without aggregation, while Nasrollahzadeh et al. described similar outcomes [42]. Elhambakhsh et al. presented the size of magnetic nanoparticles in the range of 10–33 nm [43]. Also, similar morphologies were obtained by Ayed et al. [44].

Table 3 Results of EDX analysis of synthesized nanoparticles

Element	W (%)	A (%)
Fe_3O_4		
O	29.10	58.89
Fe	70.90	41.11
Fe_3O_4@SiO_2		
O	35.02	62.21
Fe	55.58	28.28
Si	9.40	9.51
Fe_3O_4@SiO_2-NH_2		
O	47.81	69.28
Fe	38.55	16.00
Si	9.47	7.82
N	4.17	6.90

VSM

The Magnetic behavior of synthesized nanoparticles was examined by the application of VSM analysis at room temperature (Fig. 10). The suitable conditions for reaching a superparamagnetic behavior were related to the size of the nanoparticles, which needed to be between 30 and 50 nm and be lower than the superparamagnetic critical size [45]. The saturation magnetization (Ms) values of Fe_3O_4, Fe_3O_4@SiO_2 core-shell, and Fe_3O_4@SiO_2-NH_2 nanoparticles were 64, 55, and 37 emu. g^{-1} respectively. There were no values of remanence magnetization (Mr) and coercivity (Hc) detected thru the nanoparticles. The Ms values of Fe_3O_4@SiO_2 core-shell and Fe_3O_4@SiO_2-NH_2 nanoparticles were slightly decreased after the manufacture of core-shell and surface modification of nanoparticles, which could be approved to the magnetic nature of the compounds [46]. The results of our work were in agreement with the work of Pei et al. which exhibited superparamagnetic behavior [47]. Also, The outcomes are similar to Zhang et al. [48].

Evaluation of neurotoxicity effect

In the current study, 3-(4, 5-dimethylthiazol-2-yl)-2, 5-diphenyltetrazolium bromide (MTT) test was applied to examine the cytotoxicity influence of Fe_3O_4, Fe_3O_4@SiO_2 core-shell, and Fe_3O_4@SiO_2-NH_2 nanoparticles on CT-26 cell lines [49, 50]. For this aim, 100 uL of culture medium were treated in each well of a 96-well plate via different concentrations of nanoparticles (1, 10, 25, 50, 100, 200, and 400 µg mL^{-1}) to be incubated for 48 h [51]. Then, 40 µL of MTT solution (5 mg mL^{-1}) was added to assess the cell viability and was incubated for 4 h at 37 °C. To continue, 100 µL of DMSO was blended into each well to dissolve the formazan crystals. Afterward incubation, the absorbance was evaluated by the usage of a microplate reader at λ_{max} =

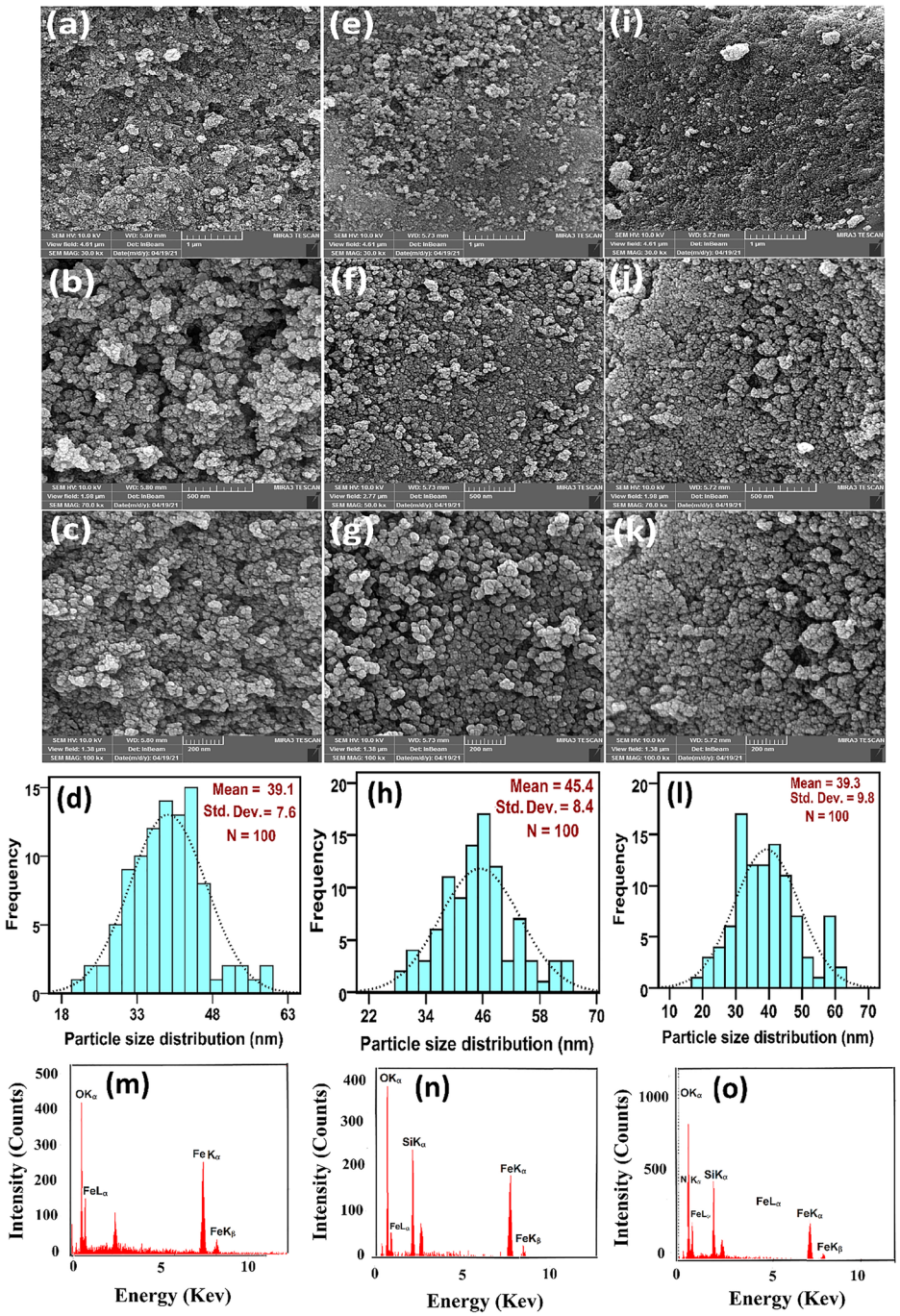

Fig. 9 The FESEM images (**a**-**k**) and PSA (**d**-**l**), and EDAX (**m**-**o**) of synthesized nanoparticles

570 nm. In end, the viability (%) was calculated by the usage of the following Eq. 10 [52].

$$\text{Viability}(\%) = \frac{\text{Abs}_{\text{test}}}{\text{Abs}_{\text{control}}} \times 100 \quad (10)$$

The outcomes have shown that the viability decreased at concentrations above 50 µg mL^{-1}, and the half-maximal inhibitory concentration (IC_{50}) values of Fe_3O_4, Fe_3O_4@SiO_2 core-shell, and Fe_3O_4@SiO_2-NH_2 nanoparticles were reported at about 50, 100, and 100 µg mL^{-1} respectively. The results of MTT assay nanoparticles on the CT-26 cell line were presented in Fig. 11. In the cytotoxicity studies, viability decreasing was observed for bare Fe_3O_4 compared to Fe_3O_4@SiO_2 and Fe_3O_4@SiO_2-NH_2 nanoparticles. Here, coating and functionalization improve the biocompatibility nature of nanoparticles, which makes them a suitable contender. Overall, Fe_3O_4@SiO_2 and Fe_3O_4@SiO_2-NH_2 nanoparticles can act as a radiosensitizer in radiotherapy which may promote new opportunities for progress in cancer

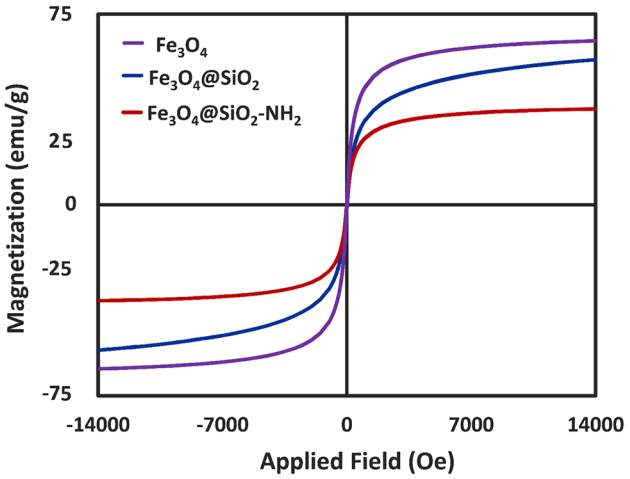

Fig. 10 Hysteresis loops of synthesized nanoparticles

radiotherapy to improve clinical efficacy in various cancer. According to obtained results, synthesized nanoparticles significantly prevented the growth of cancer cells in low concentrations. Zhang et al. 2017, reported the anticancer effect of magnetic microspheres against the Hela cells and showed that when cells are exposed to nanoparticles, was decreases cell viability [53, 54]. The use of magnetic nanoparticles was increased as anticancer drugs for treatment, which leads to the study of nanoparticles and their widespread uses. Therefore, the use of nanoparticles can be a novel method in the cure of cancer patients [55]. The importance of the present study became more apparent in vitro studies by considering the undeniable inhibitory effect of these nanoparticles [56, 57]. In addition, no side effects have been reported after the use of these nanoparticles during previous research. The study of Zhang et al. has not shown any complications or negative results on human health [58].

Conclusion

In this work, Fe_3O_4, Fe_3O_4@SiO_2 core-shell, and Fe_3O_4@SiO_2-NH_2 nanoparticles were prepared successfully by the co-precipitation method, followed by surface modification. XRD, FESEM, and EDX were utilized to distinguish the microstructure and shape of the nanoparticles. The existence of functional groups was approved by FT-IR analysis. FESEM images showed that the morphology of nanoparticles was shaped spherically. As a result, surface-modified nanoparticles may be applied for biomedical applications or as photocatalysts for pollutant degradation and other applications. The photocatalytic outcomes have shown that Fe_3O_4@SiO_2-NH_2 nanoparticles were suitable as a photocatalyst in MB dye degradation below UVA light. The degradation percentage of MB dye by the usage of Fe_3O_4@SiO_2-NH_2 nanoparticles in optimum conditions was about 90% (pH:11, catalyst concentration:10.0 mg L^{-1}, and the concentration of MB:1.0 mg L^{-1} after 150 min. The obtained outcomes propose that Fe_3O_4@SiO_2-NH_2 nanoparticles are a new photocatalyst with high efficiency for the removal of organic wastewater. Also, the cytotoxicity of Fe_3O_4, Fe_3O_4@SiO_2 core-shell, and Fe_3O_4@SiO_2-NH_2 nanoparticles was investigated on the CT-26 cell line by

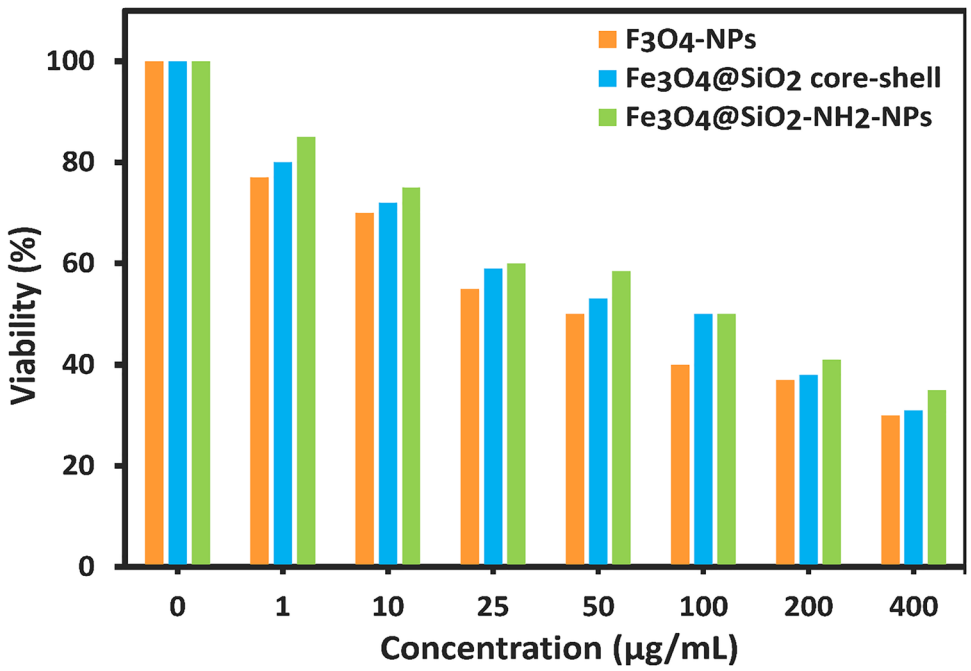

Fig. 11 Cell cytotoxicity of Fe_3O_4, Fe_3O_4@SiO_2 core-shell, and Fe_3O_4@SiO_2-NH_2 nanoparticles after 48 h of incubation on CT-26 cell lines

an MTT test and the IC_{50} values were reported at about 50, 100, and100 µg mL^{-1} respectively.

Acknowledgements This project was financially supported by the Vice-Chancellor for Research (Grant no. 4000215), Mashhad University of Medical Sciences. This study is the result of a research project and thesis presented by a Post-Doctoral student (Dr. Z. Sabouri).

CRediT authorship contribution statement Zahra Sabouri: Investigation, Methodology, Software, Writing - original draft, Formal analysis.

Mohammad Sabouri: Data curation, Formal analysis, Software, Writing - review & editing.

Samaneh Sadat Tabrizi Hafez Moghaddas: Data curation, Formal analysis, Software, Writing - review & editing.

Majid Darroudi: Supervision, Project administration, Validation, Methodology, Writing - review & editing.

Funding This project was financially supported by the Vice-Chancellor for Research (Grant no. 4000215), Mashhad University of Medical Sciences.

Data availability Not applicable.

Declarations

Consent to participate Not applicable.

Consent for publication I, the undersigned, give my consent for the publication of identifiable details, which can include a photograph(s) and/ or case history and/or details within the text ("Material") to be published in the above Journal and Article.

Competing interests Not applicable.

Research involving human participants and/or animals This article does not contain any studies with human participants or animals performed by any of the authors.

Informed consent Not applicable.

Disclosure of potential conflicts of interest The authors declare that they have no conflict of interest.

References

1. Kumar B, Smita K, Cumbal L, Debut A, Galeas S, Guerrero VH. Phytosynthesis and photocatalytic activity of magnetite (Fe3O4) nanoparticles using the Andean blackberry leaf. Mater Chem Phys. 2016;179:310–5.
2. Villegas VAR, Ramírez JIDL, Guevara EH, Sicairos SP, Ayala LAH, Sanchez BL. Synthesis and characterization of magnetite nanoparticles for photocatalysis of nitrobenzene. J Saudi Chem Soc. 2020;24(2):223–35.
3. Rahmani R, Gharanfoli M, Gholamin M, Darroudi M, Chamani J, Sadri K. Green synthesis of 99mTc-labeled-Fe3O4 nanoparticles using quince seeds extract and evaluation of their cytotoxicity and biodistribution in rats. J Mol Struct. 2019;1196:394–402.
4. Sun L, Li Y, Sun M, Wang H, Xu S, Zhang C, Yang Q. Porphyrin-functionalized Fe3O4@ SiO2 core/shell magnetic colorimetric material for detection, adsorption and removal of Hg2 + in aqueous solution. New J Chem. 2011;35(11):2697–704.
5. Amara D, Felner I, Nowik I, Margel S. Synthesis and characterization of Fe and Fe3O4 nanoparticles by thermal decomposition of triiron dodecacarbonyl. Colloids Surf A. 2009;339(1–3):106–10.
6. Ling W, Wang M, Xiong C, Xie D, Chen Q, Chu X, Qiu X, Li Y, Xiao X. Synthesis, surface modification, and applications of magnetic iron oxide nanoparticles. J Mater Res. 2019;34(11):1828–44.
7. Gholoobi A, Abnous K, Ramezani M, Shandiz FH, Darroudi M, Ghayour-Mobarhan M, Meshkat Z. Synthesis of γ-Fe 2 O 3 nanoparticles capped with oleic acid and their magnetic characterization. Iran J Sci Technol Trans A: Sci. 2018;42(4):1889–93.
8. Wang J, Zheng S, Shao Y, Liu J, Xu Z, Zhu D. Amino-functionalized Fe3O4@ SiO2 core-shell magnetic nanomaterial as a novel adsorbent for aqueous heavy metals removal. J Colloid Interface Sci. 2010;349(1):293–9.
9. Khalil M, Aulia G, Budianto E, Mohamed Jan B, Habib SH, Amir Z, Abdul Patah MF. Surface-functionalized superparamagnetic nanoparticles (SPNs) for enhanced oil recovery: Effects of Surface Modifiers and their architectures. ACS Omega. 2019;4(25):21477–86.
10. Aslani E, Abri A, Pazhang M. Immobilization of trypsin onto Fe3O4@ SiO2–NH2 and study of its activity and stability. Colloids Surf B. 2018;170:553–62.
11. Tabasi H, Hamed Mosavian MT, Sabouri Z, Khazaei M, Darroudi M. pH-responsive and CD44-targeting by Fe3O4/MSNs-NH2 nanocarriers for oxaliplatin loading and colon cancer treatment. Inorg Chem Commun. 2021;125:108430. https://doi.org/10.1016/j.inoche.2020.108430.
12. Ganapathe LS, Mohamed MA, Mohamad Yunus R, Berhanuddin DD. Magnetite (Fe3O4) nanoparticles in biomedical application: from synthesis to surface functionalization. Magnetochemistry. 2020;6(4):68.
13. Yang NQ, Li J. Improve photocatalytic performance of ZnO through coordination of ZnO/ZnIn2S4 heterojunction and graphene oxide. Eur Phys J Plus. 2021;136(9):1–11.
14. Ali A, Hira Zafar MZ, ul Haq I, Phull AR, Ali JS, Hussain A. Synthesis, characterization, applications, and challenges of iron oxide nanoparticles. Nanatechnol Sci Appl. 2016;9:49.
15. Zhu N, Ji H, Yu P, Niu J, Farooq M, Akram MW, Udego I, Li H, Niu X. Surface modification of magnetic iron oxide nanoparticles. Nanomaterials. 2018;8(10):810.
16. Tabasi H, Mosavian MTH, Darroudi M, Khazaei M, Hashemzadeh A, Sabouri Z. Synthesis and characterization of amine-functionalized Fe3O4/Mesoporous silica nanoparticles (MSNs) as potential nanocarriers in drug delivery systems. J Porous Mater. 2022. https://doi.org/10.1007/s10934-022-01259-5.
17. Chekalil N, Tarhini M, Elaissari A, Saïdi-Besbes S. Multi-step synthesis of core-shell magnetic nanoparticles bearing acid-chelating functional moieties. Res Chem Intermed. 2019;45(10):4847–61. https://doi.org/10.1007/s11164-019-03868-3.
18. Ghasemzadeh MA, Abdollahi-Basir MH, Babaei M. Fe3O4@ SiO2–NH2 core-shell nanocomposite as an efficient and green catalyst for the multi-component synthesis of highly substituted chrome no [2, 3-b] pyridines in aqueous ethanol media. Green Chem Lett Rev. 2015;8(3–4):40–9.
19. Soofivand F, Salavati-Niasari M. Step synthesis and photocatalytic activity of NiO/graphene nanocomposite under UV and visible light as an effective photocatalyst. J Photochem Photobiol A. 2017;337:44–53.
20. Munasir N, Kusumawati R, Kusumawati D, Supardi Z, Taufiq A, Darminto D. Characterization of Fe3O4/rGO composites from natural sources: application for dyes color degradation in aqueous solution. Int J Eng. 2020;33(1):18–27.
21. Patel K, Parangi T, Solanki G, Mishra M, Patel K, Pathak V. Photocatalytic degradation of methylene blue and crystal violet dyes under UV light irradiation by sonochemically synthesized CuSnSe nanocrystals. Eur Phys J Plus. 2021;136(7):1–17.

22. Nguyen XS, Pham TD, Tran TTT, Tung Vo H. Photo-oxidation efficient as (III) under visible light using microporous zn doped-Fe3O4 sphere. Mater Technol. 2020;35(6):335–48. https://doi.org/10.1080/10667857.2019.1682857.
23. Tu X, Zhou X, Ke S, Zeng Z. Controlled preparation of magnetically separable BiOBr/BiFeO3 heterostructures by chemical etching process with enhanced visible light photocatalytic activities and anti-photocorrosion. Mater Technol. 2021:1–12. https://doi.org/10.1080/10667857.2021.1936857.
24. Lu Y, Xu L, Liu C, Zhang Z. Synthesis and photocatalytic activity of composite magnetic photocatalyst MnxZn1-xFe2O4/α-Bi2O3. Mater Technol. 2019;34(5):301–11. https://doi.org/10.1080/10667857.2018.1554229.
25. Jiang Z, Yin X, Hao Y, Xu L, Liu C, Feng Q. Novel magnetic composite photocatalyst ZnO/Bi24O31Br10@SrFe12O19 with enhanced photocatalytic activity. Mater Technol. 2020:1–8. https://doi.org/10.1080/10667857.2020.1837543.
26. Sabouri Z, Akbari A, Hosseini HA, Hashemzadeh A, Darroudi M. Bio-based synthesized NiO nanoparticles and evaluation of their cellular toxicity and wastewater treatment effects. J Mol Struct. 2019;1191:101–9. https://doi.org/10.1016/j.molstruc.2019.04.075.
27. Wu W, Zhang S, Xiao X, Zhou J, Ren F, Sun L, Jiang C. Controllable synthesis, magnetic properties, and enhanced photocatalytic activity of spindlelike mesoporous α-Fe2O3/ZnO core–shell heterostructures. ACS Appl Mater Interfaces. 2012;4(7):3602–9.
28. Khandannasab N, Sabouri Z, Ghazal S, Darroudi M. Green-based synthesis of mixed-phase silver nanoparticles as an effective photocatalyst and investigation of their antibacterial properties. J Mol Struct. 2019:127411.
29. Sabouri Z, Fereydouni N, Akbari A, Hosseini HA, Hashemzadeh A, Amiri MS, Kazemi Oskuee R, Darroudi M. Plant-based synthesis of NiO nanoparticles using salvia macrosiphon Boiss extract and examination of their water treatment. Rare Met. 2020;39(10):1134–44. https://doi.org/10.1007/s12598-019-01333-z.
30. Chen Z, Yao J, Ma B, Liu B, Kim J, Li H, Zhu X, Zhao C, Amde M. A robust biocatalyst based on laccase immobilized superparamagnetic Fe3O4@SiO2–NH2 nanoparticles and its application for degradation of chlorophenols. Chemosphere. 2022;291:132727. https://doi.org/10.1016/j.chemosphere.2021.132727.
31. Jazini Zadeh R, Sayadi M, Rezaei MR. Removal of 2,4-dichlorophenoxyacetic acid from aqueous solutions by modified magnetic nanoparticles with amino functional groups. J Water Environ Nanatechnol. 2020;5(2):147–56. https://doi.org/10.22090/jwent.2020.02.005.
32. Ghasemzadeh MA, Abdollahi-Basir MH. Fe3O4@ SiO2-NH2 nanocomposite as a robust and effective catalyst for the one-pot synthesis of polysubstituted dihydropyridines. Acta Chim Slov. 2016;63(3):627–37.
33. Ali Ghasemzadeh M, Elyasi Z, Azimi-Nasrabad M, Mirhosseini-Eshkevari B. Magnetite nanoparticles-supported APTES as a powerful and recoverable nanocatalyst for the Preparation of 2-Amino-5, 10-dihydro-5, 10-dioxo-4H-benzo [g] chromenes and tetrahydrobenzo [g] quinoline-5, 10-diones. Comb Chem High Throughput Screen. 2017;20(1):64–76.
34. Smulders S, Ketkar-Atre A, Luyts K, Vriens H, De Sousa Nobre S, Rivard C, Van Landuyt K, Baken S, Smolders E, Golanski L, Ghosh M, Vanoirbeek J, Himmelreich U, Hoet PH. Body distribution of SiO2–Fe3O4 core-shell nanoparticles after intravenous injection and intratracheal instillation. Nanotoxicology. 2016;10(5):567–74. https://doi.org/10.3109/17435390.2015.1100761.
35. Zhang Y, Zhang Q, Che EX, Xia DD, Liu YC, Li D, Zhang ZD, Wang SL. A novel magnetic mesoporous silicon composite combining the function of magnetic target drug delivery and magnetic-induction hyperthermia. Mater Technol. 2015;30(sup8):B211-5. https://doi.org/10.1179/17535557B15Y.000000010.
36. Prabu D, Senthil Kumar P, Indraganti S, Sathish S, Aravind Kumar J, Vijai Anand K. One-step fabrication of amino-functionalized Fe3O4@ SiO2 core-shell magnetic nanoparticles as a potential novel platform for removal of Cadmium (II) from aqueous solution. Sustainability. 2022;14(4):2290.
37. Xu J, Ju C, Sheng J, Wang F, Zhang Q, Sun G, Sun M. Synthesis and characterization of magnetic nanoparticles and its application in lipase immobilization. Bull Korean Chem Soc. 2013;34(8):2408–12.
38. Hui C, Shen C, Tian J, Bao L, Ding H, Li C, Tian Y, Shi X, Gao H-J. Core-shell fe 3 O 4@ SiO 2 nanoparticles synthesized with well-dispersed hydrophilic Fe 3 O 4 seeds. Nanoscale. 2011;3(2):701–5.
39. Ghaderi RS, Adibian F, Sabouri Z, Davoodi J, Kazemi M, Amel Jamehdar S, Meshkat Z, Soleimanpour S, Daroudi M. Green synthesis of selenium nanoparticle by Abelmoschus esculentus extract and assessment of its antibacterial activity. Mater Technol. 2022;37(10):1289–97. https://doi.org/10.1080/10667857.2021.1935602.
40. Zhao X, Zhao H, Yuan H, Lan M. Multifunctional superparamagnetic Fe3O4@ SiO2 core/shell nanoparticles: design and application for cell imaging. J Biomed Nanotechnol. 2014;10(2):262–70.
41. Asab G, Zereffa EA, Abdo Seghne T. Synthesis of silica-coated Fe3O4 nanoparticles by microemulsion method: Characterization and evaluation of antimicrobial activity. Int J Biomater. 2022;2020:4783612. https://doi.org/10.1080/10667857.2021.1935602.
42. Nasrollahzadeh M, Sajjadi M, Khonakdar HA. Synthesis and characterization of novel Cu(II) complex coated Fe3O4@SiO2 nanoparticles for catalytic performance. J Mol Struct. 2018;1161:453–63. https://doi.org/10.1016/j.molstruc.2018.02.026.
43. Elhambakhsh A, Keshavarz P. Investigation of carbon dioxide absorption using different functionalized Fe3O4 magnetic nanoparticles. Energy Fuels. 2020;34(6):7198–208. https://doi.org/10.1021/acs.energyfuels.0c00234.
44. Ayed RB, Ajili M, Thamri A, Kamoun NT, Abdelghani A. Substrate temperature effect on the crystal growth and optoelectronic properties of sprayed α-Fe2O3 thin films: application to gas sensor and novel photovoltaic solar cell structure. Mater Technol. 2018;33(12):769–83. https://doi.org/10.1080/10667857.2018.1503385.
45. Pradhan P, Sarma HD, Mishra K, Banerjee R. Comparative evaluation of heating ability and biocompatibility of different ferrite-based magnetic fluids for hyperthermia application. J Biomed Mater Res B Appl Biomater. 2007;81(1):12–22. https://doi.org/10.1002/jbm.b.30630.
46. Yew YP, Shameli K, Miyake M, Khairudin NBBA, Mohamad SEB, Naiki T, Lee KX. Green biosynthesis of superparamagnetic magnetite Fe3O4 nanoparticles and biomedical applications in targeted anticancer drug delivery system: a review. Arab J Chem. 2020;13(1):2287–308.
47. Pei Y, Han Q, Tang L, Zhao L, Wu L. Fabrication and characterisation of hydrophobic magnetite composite nanoparticles for oil/water separation. Mater Technol. 2016;31(1):38–43. https://doi.org/10.1179/1753555715Y.0000000024.
48. Wu F, Sun B, Chu X, Zhang Q, She Z, Song S, Zhou N, Zhang J, Yi X, Wu D, Wang J. Hyaluronic acid-modified porous carbon-coated Fe3O4 nanoparticles for magnetic resonance imaging-guided photothermal/chemotherapy of tumors. Langmuir. 2019;35(40):13135–44. https://doi.org/10.1021/acs.langmuir.9b02300.
49. Chen D, Tang Q, Li X, Zhou X, Zang J, Xue W-q, Xiang J-y, Guo C-q. Biocompatibility of magnetic Fe3O4 nanoparticles and their cytotoxic effect on MCF-7 cells. Int J Nanomed. 2012;7:4973.

50. Liu D, Li X, Chen C, Li C, Zhou C, Zhang W, Zhao J, Fan J, Cheng K, Chen L. Target–specific delivery of oxaliplatin to HER2–positive gastric cancer cells in vivo using oxaliplatin–au–fe3o4–herceptin nanoparticles. Oncol Lett. 2018;15(5):8079–87.
51. Mosmann T. Rapid colorimetric assay for cellular growth and survival: application to proliferation and cytotoxicity assays. J Immunol Methods. 1983;65(1–2):55–63.
52. van Meerloo J, Kaspers GJ, Cloos J. Cell sensitivity assays: the MTT assay. In: Cancer cell culture. Springer; 2011. pp. 237–45.
53. Zhang X, Xu M, Zhang Z, Hu X, Hao L, Lin Q, Wang S, Jiang W. Preparation and characterization of magnetic fluorescent microspheres for delivery of kaempferol. Mater Technol. 2017;32(3):125–30. https://doi.org/10.1080/10667857.2016.1157913.
54. Li J, Zhang J, Guo Z, Jiang H, Zhang H, Wang X. Self-assembly fabrication of honeycomb-like magnetic–fluorescent Fe3O4–QDs nanocomposites for Bimodal Imaging. Langmuir. 2020;36(48):14471–7.
55. Zhang XJ, Cai WB, Hao LY, Hu XH, Wei XJ, Wang XY, Lin Q. Preparation of thermo/pH-sensitive reduced graphene oxide interpenetrating hydrogel nanocomposites for co-delivery of paclitaxel and epirubicin. Mater Technol. 2018;33(4):245–52. https://doi.org/10.1080/10667857.2017.1410987.
56. Guo Q, Kong F, Ma C, Cao H. Preparation of doxorubicin loaded poly(ethylene glycol)-Poly(ε-caprolactone)-hydroxyapatite fibres as drug delivery systems. Mater Technol. 2020;35(4):203–11. https://doi.org/10.1080/10667857.2019.1674477.
57. Mostafapour A, Baharara J, Khazaei M, Avan A, Hassanian SM. The angiotensin-converting enzyme inhibitor 'Enalapril' increases the anti-proliferative activity of 5-Fluorouracil in Colorectal Cancer cells. Eurasian J Med Oncol. 2021;5(4):318–26.
58. Jiang P, Zhang Y, Zhu C, Zhang W, Mao Z, Gao C. Fe3O4/BSA particles induce osteogenic differentiation of mesenchymal stem cells under static magnetic field. Acta Biomater. 2016;46:141–50. https://doi.org/10.1016/j.actbio.2016.09.020.